

Conformational Equilibria of Bulged Sites in Duplex DNA Studied by EPR Spectroscopy[†]

Alyssa L. Smith,[‡] Pavol Cekan,[§] Greg P. Brewwood,^{||} Tamara M. Okonogi,^{‡,⊥} Saba Alemayehu,^{||}
Eric J. Hustedt,[#] Albert S. Benight,^{||,∇} Snorri Th. Sigurdsson,[§] and Bruce H. Robinson^{*,‡}

Department of Chemistry, University of Washington, Box 351700 Bagley Hall,
Seattle, Washington 98195-1700, University of Iceland, Science Institute, Dunhaga 3, 107 Reykjavik, Iceland,
Portland Bioscience, Inc., Portland, Oregon 97201, Fleming Pharmaceuticals, 1733 Gilsinn Lane,
Fenton, Missouri 63026, Molecular Physiology and Biophysics and Center for Structural Biology, Vanderbilt
University, Nashville, Tennessee 37232, and Department of Physics and Department of Chemistry, Portland
State University, Portland, Oregon 97207

Received: September 16, 2008; Revised Manuscript Received: December 9, 2008

Conformational flexibility in nucleic acids provides a basis for complex structures, binding, and signaling. One-base bulges directly neighboring single-base mismatches in nucleic acids can be present in a minimum of two distinct conformations, complicating the examination of the thermodynamics by calorimetry or UV-monitored melting techniques. To provide additional information about such structures, we demonstrate how electron paramagnetic resonance (EPR) active spin-labeled base analogues, base-specifically incorporated into the DNA, are monitors of the superposition of different bulge-mismatch conformations. EPR spectra provide information about the dynamic environments of the probe. This information is cast in terms of “dynamic signatures” that have an underlying basis in structural variations. By examining the changes in the equilibrium of the different states across a range of temperatures, the enthalpy and entropy of the interconversion among possible conformations can be determined. The DNA constructs with a single bulge neighboring a single-base mismatch (“bulge-mismatches”) may be approximately modeled as an equilibrium between two possible conformations. This structural information provides insight into the local composition of the bulge-mismatch sequences. Experiments on the bulge-mismatches show that basepairing across the helix can be understood in terms of purine and pyrimidine interactions, rather than specific bases. Measurements of the enthalpy and entropy of formation for the bulge-mismatches by differential scanning calorimetry and UV-monitored melting confirm that the formation of bulge-mismatches is in fact more complicated than a simple two-state process, consistent with the base-specific spectral data that bulge-mismatches exist in multiple conformations in the premelting temperature region. We find that the calculations with the nearest-neighbor (NN) model for the two likely conformations do not correlate well with the populations of structures and thermodynamic parameters inferred from the base-specific EPR dynamics probe. We report that the base-specific spin probes are able to identify a bistable, temperature dependent, switching between conformations for a particular complex bulged construct.

Introduction

DNA sequence dependent structure is extremely polymorphic. Depending upon the particular sequences comprising two strands, there are a number of alternate possible minor structures that can coexist due to favorable sequence dependent interactions. Such minor duplex structures might contain mismatch base pairs, bulged base pairs, or other non-Watson–Crick interactions within the duplexes. Consequently, depending on their sequences, a population of duplex complexes can occupy multiple conformations that may be separated by relatively small energy barriers and therefore may interconvert resulting in a steady-state of multiple duplex conformations. Such manifold minor duplex structures with small energy barriers between them

have been suggested for over twenty years,^{1–6} although their characterization has been elusive. EPR spectroscopy provides an ideal tool with which to probe existence and interconversion of multiple interdependent conformers in the premelting region in regions where bulged and mismatched bases are found.

Extrahelical (bulged) bases can be vital to the structure and function of RNA and DNA systems or to sources of potentially harmful frame-shift or deletion mutations. Only 1.2% of human DNA codes for proteins, leaving a vast amount of DNA, much of which is nonduplexed.⁷ One nonduplex, noncoding sequence neighbors the human pseudoautosomal telomere and is composed of a loop made of neighboring mismatched bases.⁸ This looped type of nonduplex structure has been postulated to serve as a molecular switch and is but one example of how noncoding DNA influences biological function.⁹

Bulges are often intermediates for errors in DNA replication, targets for repair enzymes in imperfect homologous recombination,¹⁰ and are believed to play a significant role in many diseases, including muscular dystrophy and Alzheimer’s.^{11,12} In fact, single-nucleotide polymorphisms (SNPs), which include some forms of single-base bulges, are thought to account for ~90% of mutations in an individual’s DNA.¹³ There is much

[†] Part of the “J. Michael Schurr Special Section”.

* To whom correspondence should be addressed. E-mail: robinson@chem.washington.edu. Phone: (206) 543-1773. Fax: (206) 616-6250.

[‡] University of Washington.

[§] University of Iceland.

^{||} Portland Bioscience, Inc.

[⊥] Fleming Pharmaceuticals.

[#] Vanderbilt University.

[∇] Portland State University.

68 interest in developing high-throughput SNP detection methods
69 in order to map diseases and disease susceptibility to a set of
70 SNPs. New techniques to probe for SNPs are being developed,
71 which require an understanding of the structure and dynamics
72 of SNP sites.^{14–18} Sequence-dependent effects have a profound
73 impact on the insertion or deletion of bases during DNA
74 replication and could determine the type and severity of an
75 SNP.¹⁹ It has been shown that the frequency of one-base deletion
76 mutations are affected by the identity of the base as well as of
77 its neighboring bases.²⁰

78 A number of studies have indicated that bulge structure and
79 dynamics are size, sequence, position, and temperature dependent.^{21–28}
80 For example, solution NMR studies have shown that for
81 thymidine or cytidine bulges, the position of the bulge relative
82 to the helix depends on both temperature and flanking
83 sequence.^{21,22} To understand the energetics underlying the
84 structure and sequence-dependent structure of duplex DNAs,
85 UV-monitored melting is often employed. While experimentally
86 straightforward, a shortcoming of this technique is that results
87 are ordinarily analyzed assuming DNA hybridizes in a two-
88 state manner. For many DNA sequences, it is unlikely that
89 melting is simply a transition between two well-defined
90 structures. Even so, the two-state assumption is often employed
91 in the analysis of DNA melting curves collected by UV
92 absorbance and the evaluation of thermodynamic parameters.
93 The two-state model is particularly inadequate for DNA systems
94 with conformational flexibility that can exist in multiple distinct
95 structures prior to melting. In contrast to UV melting, differential
96 scanning calorimetry (DSC) is commonly used to determine the
97 enthalpy and entropy of formation of a nucleic acid in a model-
98 independent manner. By combining the DSC and UV melting
99 results, it can be determined whether the DNA actually melts
100 in a two-state manner.²⁹

101 The most widely used method to predict the thermodynamics
102 of the melting transition for a given DNA sequence is the
103 nearest-neighbor (NN) model. First developed by Crothers et
104 al. and Tinoco et al.,^{30,31} the NN model assumes that the
105 thermodynamics of a duplex with known sequence can be
106 calculated as the sum of individual NN doublets comprising
107 the specific sequence. In the NN model, sequence dependence
108 or other types of interactions are implicitly assumed not to
109 extend beyond two base pairs. SantaLucia evaluated and
110 reported a “unified” set of NN parameters for perfectly matched
111 duplexes.³² Since being reported, these unified parameters have
112 been ubiquitously applied to the design of DNA probes and
113 primers. NN parameters are also available for all possible single-
114 base pair mismatches, and single base overhangs. In contrast,
115 comparatively few groups have studied in any systematic way
116 the consequences on thermodynamic properties of duplex DNAs
117 containing a single base bulge flanked by a mismatch base pair.
118 Because of lack of availability of quantitative parameters, current
119 applications of the NN model either ignore the bulge or assume
120 it to behave as a broken base pair.

121 Each of the DNA constructs in this study is composed of a
122 short oligomer containing a single spin-labeled base. The same
123 spin-labeled oligomer is then hybridized with various nonlabeled
124 complementary oligomers, each one base shorter than the spin-
125 labeled oligomer. At minimum, the resulting structure is
126 composed of two conformations capable of interconversion.
127 These “bulge-mismatch” constructs are compared to two refer-
128 ence spectra: the EPR spectra of the spin-labeled bases within
129 fully duplexed DNAs are the reference spectra reflecting
130 minimum base motion, and the EPR spectra of DNAs containing
131 a spin-labeled base with no available partner are the reference

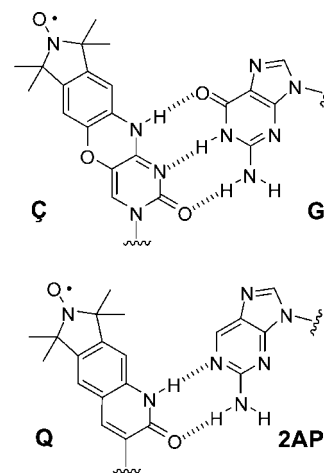


Figure 1. Structure of spin labels. Top: **C** shown paired to **G**. Bottom: **Q** shown paired to 2-aminopurine (**2AP**).

132 spectra reflecting maximum base motion. The EPR spectra
133 contain information of the dynamics of the spin probe, which
134 in turn is information about the local structure of the DNA
135 around the spin probe. The spin label within the constructs
136 reflects either rapid or slow motion depending on whether the
137 environment allows the probe to move with respect to the DNA
138 or whether the environment hinders that motion. In this way,
139 the multiplicity of spin probe environments reflects the equi-
140 librium among possible structures. The EPR-based information
141 is complementary to standard thermodynamic data because it
142 indicates which possible structures are present within a single
143 thermodynamic state. Additionally, we report that DSC studies
144 on the same constructs support the notion that multiple structures
145 are present at all temperatures.

146 Materials and Methods

147 **DNA Samples.** DNA oligomers were constructed through
148 solid-state synthesis, as described elsewhere.^{33–35} For all experi-
149 ments, samples were prepared in a solvent of 10 mM sodium
150 phosphate, 100 mM sodium chloride, and 0.1 mM EDTA at
151 pH 7.0 buffer (PNE buffer).

152 **Samples for EPR Studies.** In this study, spin labels **C** and **Q**
153 were employed. The structures are shown in Figure 1 where **C**
154 is an analog of cytosine and forms a Watson–Crick-like base
155 pair with **G**, and **Q** forms a base pair with 2-amino purine (**2AP**).
156 Spin labels were incorporated into the duplex constructs called
157 **G**C**C**G**/G**, **G**C**T**, **G**Q**P**, **Q**A**P**, **G**C**A**, **Q**A**C**, and **G**C**A/AC**
158 displayed in Figure 2. Control duplexes containing spin labels,
159 and referred to as constructs **I–VI**, are shown in Figure 3. To
160 make the duplexes shown in Figures 2 and 3, the spin-labeled
161 sequences were combined in a 1:1.2–1.5 ratio with the
162 appropriate unlabeled complementary strand and hybridized
163 stepwise on a thermocycler according to the following scheme:
164 90 °C, 2 min; 60 °C, 5 min; 50 °C, 5 min; 40 °C, 5 min; 22 °C,
165 15 min; store at 4 °C. Sequence design was such that the bulge
166 constructs contained one less nucleotide on the unlabeled strand
167 than the spin-labeled strand to create a one-base bulge on the
168 spin-labeled strand of the hybridized duplex. Sample labels
169 indicate the bases on the longer strand, 5' to 3', followed by
170 the base(s) on the shorter strand. For the EPR experiments, the
171 final concentration of the spin-labeled DNA was between 80
172 and 150 μM.

173 **Samples for DSC and UV Melting.** DNA concentrations were
174 3.6 μM for UV melting experiments performed on the com-
175 plexes shown in Figures 2 and 3. DNA samples for DSC melting

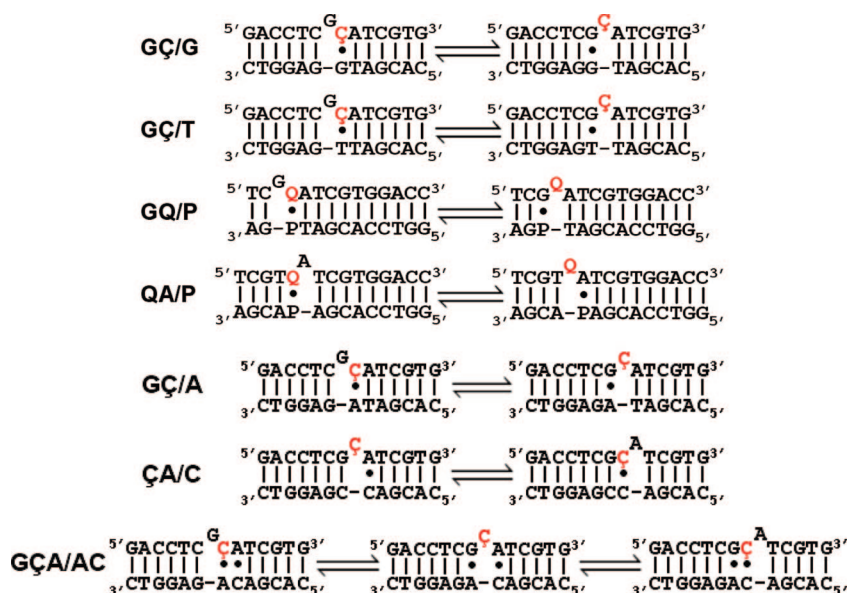


Figure 2. Samples for the bulge/single-mismatch equilibria experiments studied in this work. Each is shown in its two likely conformations, as an equilibrium between spin label SLOW (the first conformation shown in each equilibrium) and FAST (the second conformation). The red font is used at the position of the spin probe, which for **GÇ/G**, **GÇ/T**, **GÇ/A**, and **ÇA/C** is **Ç** and **GQ/P** and **QA/P** is **Q**. Vertical black lines represent Watson–Crick basepairs, and black dots represent non-Watson–Crick pairings. **P** represents 2-aminopurine, the basepairing partner for the spin label used in samples **GQ/P** and **QA/P**. The doubly mismatched, bulged sample is **GÇA/AC**. The spin probe **Ç** is indicated in red font, black lines represent Watson–Crick basepairs, and black dots represent non-Watson–Crick pairings. The two conformations for the double-mismatch sample are indicated by **GÇ/A** and **ÇA/C**, which represent the two likely possible equilibria of the same sample.



Figure 3. Control SLOW (left) and FAST (right) samples for the bulge/single-mismatch equilibria experiments. Each of the SLOW controls has the spin label locked into the duplex structure, and each of the FAST controls has Watson–Crick basepairs on each side of the spin label with no partner provided for the spin probe itself. The spin probe is indicated in each construct by red font, and **P** represents **Q**'s basepairing partner, 2-aminopurine. The top sample of each column (I and IV) is the control for **GÇ/G** and **GÇ/T**, the constructs II and V are the SLOW and FAST controls for **GQ/P**, and III and VI are controls for **QA/P**. UV monitored T_{Ms} are given in Table 1.

experiments were analogous to those used for EPR studies and UV melting, except a natural cytidine replaced the spin probe analog, **Ç**, because of the large sample volumes for DSC measurements. For DSC melting experiments, duplex DNA concentrations were 75–130 μM .³³

UV-Monitored Melting Experiments. Absorbance at 268 nm versus temperature measurements (UV melting curves) were collected using a Cary 100 UV–vis spectrophotometer (Varian Instruments, Walnut Creek, CA). Sample temperature was increased from 10 to 80 °C at a rate of 0.5 °C/min. Data points were collected every 0.5 °C.

Differential Scanning Calorimetry Measurements. DSC melting curves were collected as measurements of the excess heat capacity, ΔC_p , versus temperature, using one of four Nano-DSC differential scanning calorimeters (Calorimetry Sciences Corp - CSC). Data was analyzed using the Cpcalc (CSC) routine and produced the melting enthalpy (ΔH_f°) and entropy (ΔS_f°). Free energy (ΔG_f°) was calculated using the formula $\Delta G_f^\circ =$

$\Delta H_f^\circ - T\Delta S_f^\circ$. For all melting experiments, DNA concentrations ranged from 75–130 mM.

EPR Experiments and Data Analysis. CW-EPR Experiments. Using a commercial X-band (~9.4 GHz) Bruker EMX EPR spectrometer, spectra were collected from 0 to 40 at 5 °C intervals, accurate to ± 0.2 °C, such that the highest temperature data point for each sample is still at least 5 °C below the UV-monitored melting temperature for that construct. For each sample, 50–100 scans were taken and averaged to obtain the final spectrum. A modulation frequency of 100 kHz at modulation amplitude 1.0 G was used, at 2.0 mW microwave power (nonsaturating conditions).

Saturation Recovery EPR Experiments. Pulsed saturation recovery (pSR) spectra were acquired at X-band (~9.2 GHz) on a home-built EPR spectrometer with both CW and saturation recovery EPR measurement capability.³⁶ A CW spectrum is obtained with resolution of 1024 points over a range of 90 G during one scan at a constantly applied –12 dbm microwave power with 1 G modulation amplitude and a modulation frequency of 10 kHz. The highest spin density point for an ¹⁴N-nitroxide-labeled DNA sample is the center of the spectrum; this position was chosen as the field position at which the pump pulse was applied for the pSR experiment. To collect data by pSR, a 200 ns pump pulse was applied with +20 dbm of microwave power, followed by a 90 ns dead time. The response was observed with an offset of 100 kHz at –12 dbm of microwave power. The typical time resolution for a pSR spectrum in this study was 20 ns per point for 4096 points and averaged over 4.8×10^6 scans (80% of the scans on resonance and 20% ~100 Gauss off resonance for background subtraction). For each relaxation rate reported, the experiment was repeated at minimum six times and the results averaged. All samples were in a gas-permeable, but not water-permeable, 0.8 mm inner diameter Teflon capillary tube under a continuous stream of N₂ gas at ~21 °C.

Dynamic Signatures from EPR Spectra. There are several ways of measuring EPR spectral features reported by a spin

176
177
178
179
180
181
182
183
184
185
186
187
188
189
190
191
192
193

194
195
196
197
198
199
200
201
202
203
204
205
206
207
208
209
210
211
212
213
214
215
216
217
218
219
220
221
222
223
224
225
226
227
228
229
230

TABLE 1: Results of UV-Monitored Measurements

sample	ΔH_f [kcal/mol]	ΔS_f [cal/mol]	$\Delta G_{f, 20}$ [kcal/mol]	T_m [°C]
FAST IV	-100.7 ± 1.4	-289 ± 4	-15.9 ± 1.6	46.8 ± 0.9
GÇ/G	-94.7 ± 2.2	-270 ± 4	-15.6 ± 2.5	47.4 ± 0.6
GÇ/T	-92.3 ± 1.4	-267 ± 4	-13.8 ± 1.6	41.2 ± 0.5
GÇ/A	-88.8 ± 2.5	-257 ± 5	-13.1 ± 2.7	40.2 ± 0.6
ÇA/C ^a	-60.3 ± 3.6	-165 ± 13	-11.9 ± 5.0	38.9 ± 0.3
GÇA/AC	-60.4 ± 3.8	-168 ± 10	-12.6 ± 5.0	33.2 ± 0.3
Ç/G	-116.3 ± 3.0	-323 ± 11	-21.6 ± 3.5	61.7 ± 0.6
Ç/T	-87.2 ± 3.1	-244 ± 10	-15.7 ± 3.6	48.6 ± 0.3
Ç/A	-89.7 ± 1.3	-250 ± 4	-16.4 ± 1.7	51.1 ± 0.5
Ç/C, SLOW I ^a	-97.4 ± 2.7	-278 ± 11	-15.9 ± 3.2	46.0 ± 0.3

^a These samples have a broadened peak, although they can still be fit by the UV melting two-state model. The values are likely less accurate.

probe and obtaining a “dynamic signature”. One method is to measure the full peak-to-trough width (referred to as $\langle 2A_{zz} \rangle$ in EPR literature) of the CW-EPR spectra.³⁷ A second method is to measure the line width of the central peak in the CW-EPR.³⁸ The third method is to directly measure the spin–lattice relaxation rate.^{36,39} As briefly described below, for each of these signatures the more exposed the labeled base is to the solvent environment, the less constrained it is by the adjoining duplex structure and therefore the faster the characteristic motional time.

1. Spectral Width, $\langle 2A_{zz} \rangle$

The peak-to-trough spectral width is measured as the difference between the maximum of the low-field peak and the minimum of the high-field peak. Standard routines within Matlab are used to search for the local maximum and minimum. Measurements are routinely repeated on at least two independently prepared samples.

2. Center Manifold Linewidth

The observed width of the center field line is obtained using Matlab to search for the maximum and minimum of the CW-EPR spectra. The line width is the difference in field positions of the minimum and maximum of the CW-EPR spectra. The extrema of the center field line are that of the full EPR spectra. The measurement was repeated on at least two independently prepared samples.

3. Spin–lattice Relaxation Rate

A set of 6–10 pSR-EPR measurements was fit globally to a single exponential, giving a single relaxation rate. A comparison was performed using two relaxation rates to demonstrate that the spectra were fit better by a single exponential decay curve.

Fitting of EPR Spectra to a Sum of Two Components. For the bulged DNA duplexes of this study, EPR spectra were modeled as the sum of two reference spectra, using a least-squares fitting routine (Marquardt–Levenberg minimization algorithm) in Matlab. At each temperature, control spectra were measured at the same temperature as the sample spectra, and the sample spectra fit as a superposition of two control spectra. All spectra were normalized, and the points of maximum intensity on the center field line in each of the spectra (where $y = 0$ in the derivative spectra) were aligned. This ensured that any variation in frequency of the instrument did not affect the results of the fitting procedure. Previous work has shown that this method was in good agreement with standard methods of determining fractions of two components in a mixture.⁴⁰

To determine errors in fitting of EPR spectra, several metrics were evaluated. Spectra for each bulge-mismatch construct were obtained at least twice on multiple samples. Spectra were digitized to 4096 points by the EPR instrument and then filtered to 256 points to facilitate computation. Even further reducing the number of points to 128 did not affect the results. Each

EPR spectrum was fit to sets of SLOW and FAST control spectra. Reducing the number of points slightly increased the errors in the Marquardt–Levenberg fitting (because the total error was averaged over fewer points).

Simulation of EPR Spectra. Simulations of EPR spectra were performed according to the methods of Freed and co-workers.⁴¹ The simulation was performed using the following tensors, derived from a fit to a rigid-limit spectra of a 14-mer DNA in 50% (w/v) sucrose/PNE solution at 0 °C (determined in a previous study): $g_{xx} = 2.0086$, $g_{yy} = 2.0064$, $g_{zz} = 2.0026$, $A_{xx} = 5.81$ G, $A_{yy} = 5.75$ G, and $A_{zz} = 36.75$ G.⁴² The homogeneous linewidths were chosen to be 0.7, 0.85, and 1.3 G (from low field to high field), and the inhomogeneous broadening function had a width of 0.58 G.⁴² The tilt of the Euler angle β was set equal to 20°. The diffusion tensor values were calculated for a rigid cylinder of the dimensions of a 14-mer DNA at differing temperatures, based on the well-established methods of Tirado and de la Torre.^{42,43}

Theoretical Methods and Data Analysis. Interconversion Between SLOW and FAST Conformations: Enthalpies and Entropies from EPR Experimental Data. The bulge-mismatch constructs were modeled assuming a two-state equilibrium between two distinct conformations of each bulge-mismatch. These states are a duplex DNA with a spin label in the bulged position (out, FAST dynamics) and a duplex with the spin label firmly locked into the duplex structure (in, SLOW conformational dynamics).⁴⁴ EPR spectra were analyzed to determine the dynamic equilibrium between the FAST and SLOW states. The middle spectrum of Figure 4 shows an example fit of a bulge-mismatch sample to spectra from the SLOW and FAST controls. The chemical reaction is two-state: $SLOW \rightleftharpoons FAST$. The control spectra from sample I (blue in Figure 4), $S(x)$, and IV (green), $F(x)$, were added to produce a least-squares fitted line (black dashed), shown superimposed on top of the target sample (red) spectrum. All spectra, $E(x)$, were normalized to unity with the double integral

$$\int_{x=-\infty}^{\infty} \int_{x'=-\infty}^x E(x') dx' dx = 1$$

$$E(x) = a_{SLOW}S(x) + a_{FAST}F(x) \quad (1.1)$$

$$a_{SLOW} + a_{FAST} = 1 \quad (1.2)$$

The expression for the equilibrium between SLOW and FAST conformations is given by

$$K_{eq} = \frac{(F)}{(S)} = \frac{a_{FAST}}{a_{SLOW}} = \frac{a_{SLOW}}{1 - a_{SLOW}} \quad (1.2)$$

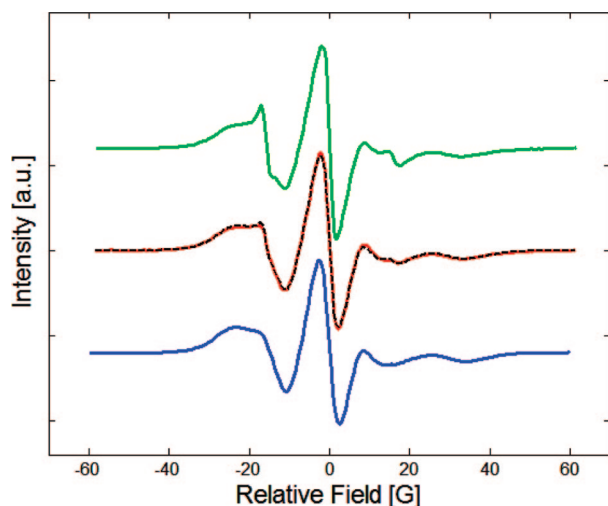


Figure 4. EPR spectrum of GÇ/T (red line), compared with the SLOW control (blue) and FAST control (green). The summed superposition of the SLOW and FAST controls is shown (dashed black line), where GÇ/T at 35 °C is fit by a sum of 38.2% control FAST at 35 °C and 61.8% SLOW at 35 °C.

To evaluate the thermodynamics of the SLOW to FAST interconversion reaction, the natural logarithm of the equilibrium constant, K_{eq} , obtained from the ratio in eq 1.2, was plotted according to the van't Hoff relation

$$\ln(K_{eq}) = -\frac{\Delta H_D}{RT} + \frac{\Delta S_D}{R} \quad (1.3)$$

The slope was $(-\Delta H_D/R)$ and the intercept $(\Delta S_D/R)$, and K_{eq} is the ratio obtained from eq 1.2. Results of the linear fits provided evaluations of ΔH_D and ΔS_D , determined by the dynamics associated with the spin probe being bulged out or locked into the helical structure. The values ΔH_D and ΔS_D were compared to analogous quantities, ΔH_{NN} and ΔS_{NN} , estimated from the NN model.

Interconversion Between Conformations: Calculation of Enthalpies and Entropies from the Unified Nearest-Neighbor (NN) Model. On the basis of the assumption that the dynamics can be approximately described in terms of a SLOW and FAST structure (used to obtain K_{eq} and ΔH_D above), the NN method can be applied to approximate $\Delta\Delta H_{NN}$ and $\Delta\Delta S_{NN}$. Calculations were based on the published NN parameters.³² For example, the calculation to determine the NN enthalpy is demonstrated. The same process is used to determine the entropy. The difference in enthalpy between the FAST and SLOW components is given by

$$\Delta\Delta H_{NN} = \left[\sum_i n_i \Delta H_f(i) \right]_{FAST} - \left[\sum_i n_i \Delta H_f(i) \right]_{SLOW} \quad (1.4)$$

For example, consider the two equilibrium states of GÇ/T, shown in Figure 2. The difference can be calculated in two ways, depending on how the mismatched and bulged bases are treated.

1. Assume the enthalpy of a bulge-mismatch construct is not affected by the presence of the bulge. This approximation allows determination of the interconversion enthalpy from the difference in energies of the different basepairs flanking the bulge in the two conformational states. After identical terms that appear

in ΔH_f for both SLOW and FAST conformations cancel, the result for $\Delta\Delta H_{NN}$ of interconversion is

$$\Delta\Delta H_{NN}(1) = [(\Delta H_{CG/GT} + \Delta H_{GA/TT}) - (\Delta H_{CC/GT} + \Delta H_{CA/TT})] \quad (1.5)$$

CG/GT represents the NN doublet (i.e., ${}^5CG^3/{}^3GT^5$), comprised of a C:G Watson-Crick basepair flanked by a G:T mismatch. This analysis omits contributions from the bulged Ç in the FAST conformation and the bulged G in the SLOW conformation.

2. Assume the contribution from the basepair adjoining the bulge can be ignored, which implicitly assumes that stacking interactions “across” the bulged site do not contribute significantly to the interconversion reaction. The result is

$$\Delta\Delta H_{NN}(2) = [\Delta H_{CG/GT} - \Delta H_{CA/TT}] \quad (1.6)$$

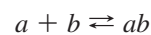
There are literature values for ΔH_{NN} and ΔS_{NN} in 1 M Na⁺. For fully duplex oligomers under 16 basepairs long, the following conversion has been employed to determine ΔS_{NN} at a lower [Na⁺]⁴⁵

$$\Delta S_{low_Na} = \Delta S_{1M_Na} + 0.386 \left(\frac{N_{phos}}{2} \right) \log[Na^+] \quad (1.7)$$

where N_{phos} is the number of phosphate groups in the oligomer, $N_{phos} = N_{length} * 2 - 2$ in basepairs, and N_{length} is the length of the oligomer in basepairs. This correction of ΔS_{NN} has not been tested for bulge-containing duplexes, although we used eq 1.7 in our calculations of ΔS_{NN} . It is reported that ΔH_f for DNA duplexes is independent of Na⁺ concentration, thus it is assumed that $\Delta\Delta H_{NN}$ for the bulge-mismatch samples is not affected by [Na⁺].⁴⁵

In the NN calculations, the Q spin probe was treated as thymidine, the 2-aminopurine as an adenosine, and the Ç spin probe as cytidine. Earlier work established that these spin probes are thermodynamically analogous to the natural bases.^{33,34,44,46} It should be noted that the NN model is based on thermodynamic parameters obtained from analysis of melting curves of duplex DNAs, even though it has been applied to estimate thermodynamic parameters below the melting region.

UV-Monitored Melting: Enthalpies and Entropies of Formation from Experimental Data. To estimate melting thermodynamic parameters from UV melting curves, the low and high temperature linear sections were extrapolated across the temperature range, as depicted in Figure S1 in Supporting Information. Procedures developed by Breslauer and co-workers were utilized to evaluate thermodynamic parameters from DNA melting curves.²⁹ In the nonlinear region, each temperature-absorbance point is defined as the fraction of strands in the duplex state, $\alpha_i = \alpha(T_i) = X/X + Y$, where the index (T_i) refers to the temperature. Determination of X and Y is shown graphically in Figure S1 in Supporting Information. The basic annealing reaction is given by



394 With $C_T = (a) + (b) + 2(ab) = 2\{(a) + (ab)\}$ (1.8)

395
$$\alpha = \frac{2(ab)}{C_T}$$

396 C_T is equal to the total strand concentration. The equilibrium
397 constant at each point i along the curve is given by

398
$$K_i = \frac{2\alpha_i}{C_T(1 - \alpha_i)^2}$$
 (1.9)

399 Melting temperature, T_m , is defined as the temperature when
400 $\alpha = 0.5$ (half of the DNA is single-stranded). The equilibrium
constant at the T_m is

401
$$K_{T_m} = \frac{4}{C_T}$$
 (1.10)

402 The standard form of the van't Hoff equation is given as

403
$$\Delta H_f = \frac{R \ln\left(\frac{K_{T_m}}{K_i}\right)}{\left(\frac{1}{T_i} - \frac{1}{T_m}\right)}$$
 (1.11)

404 To calculate the free energy at each point of the transition

405
$$\Delta G_i = -RT_i \ln(K_i)$$
 (1.12)

406 The equilibrium constant ($K_i = K(T_i)$) is for the reaction of
407 two distinct strands going to a duplex. It should correspond to
408 the relative fraction of spin label that is solvent exposed (bulged
409 out) versus locked into the duplex structure, at each temperature
(T_i) through the melting (nonlinear) region.

The entropy of the annealing reaction from single strands to
duplex is calculated using eq 1.13

409
$$\Delta S_f = \frac{\Delta H_f - \Delta G_i}{T_i}$$
 (1.13)

410 **DSC Melting: Enthalpies and Entropies of Formation from**
411 **Experimental Data.** DSC measures changes in excess heat

412 capacity, ΔC_p , versus temperature T when a DNA sample is
413 heated or cooled. Thermodynamic parameters of the DNA
414 melting transition, ΔH_{cal} and ΔS_{cal} were evaluated from the
415 normalized, baseline corrected ΔC_p versus temperature curve.^{47,48}
416 DSC data were collected at heating rates from 15 to 90 °C/hr.
417 The average buffer baseline determined from multiple (usually
418 more than eight) scans of the buffer alone was subtracted from
419 these curves. The resulting baseline corrected curve was then
420 normalized for total DNA concentration and the calorimetric
421 transition enthalpy, ΔH_{cal} , and entropy, ΔS_{cal} , are evaluated.
422 Routinely, at least three forward and reverse ΔC_p versus T scans
423 were made per experiment. For short DNA melting curves it is
424 generally assumed⁴⁹ that $\Delta C_p = \Delta C_p(T_{initial}) - \Delta C_p(T_{final}) = 0$,
425 but this assumption has not been generally validated (mainly
426 because it is difficult to measure). If there is no net excess ΔC_p
427 in the melting reaction, then the thermodynamic transition

parameters, evaluated from analysis of the transition (in the
temperature region of the transition, i.e. at T_m), were assumed
to be entirely independent of temperature. These evaluated
parameters are then applied to calculate stabilities (equilibrium
constants) of duplex complexes at temperatures below (20–40
°C) the transition region. In the few cases attempted to evaluate
 $\Delta C_p \neq 0$ for DNA melting, the derived value has been found
to be relatively small, but nonzero.^{49–52} Yet this is clearly an
issue that has not been settled. It is particularly relevant for the
interpretation of reactions that occur far below the transition
region. As in this study, small differences in thermodynamic
stability of different duplexes are introduced via sequence
specific design.

The effect of a nonzero ΔC_p on the evaluated thermodynamic
parameters is as follows

428
$$\begin{aligned} \Delta H(T) &= \Delta H^\circ(T^\circ) + \Delta C_p(T - T^\circ) \\ \Delta S(T) &= \Delta S^\circ(T^\circ) + \Delta C_p \ln\left(\frac{T}{T^\circ}\right) \end{aligned}$$
 (1.14)

429 The values of $\Delta H^\circ(T^\circ)$ and $\Delta S^\circ(T^\circ)$ are the enthalpy and
430 entropy values at the reference temperature T° , which can be
431 designated as the melting transition temperature T_m . The
432 parameters in the transition region $\Delta H^\circ(T^\circ)$ and $\Delta S^\circ(T^\circ)$ can
433 be evaluated by DSC. In practice, DSC melting curves are
434 acquired using Nano-II differential scanning calorimeters (Cal-
435 orimetry Sciences Corp., Provo, Utah). If $\Delta H^\circ(T^\circ) = \Delta H_{cal}$ and
436 $\Delta S^\circ(T^\circ) = \Delta S_{cal}$ are evaluated by DSC, and ΔC_p is known for
437 a duplex, values of $\Delta H(T)$ and $\Delta S(T)$ for melting (or annealing)
438 can be determined at any temperature and will likely be more
439 accurate.

440 **Results**

441 We report data on bulge-mismatch constructs (Figure 2),
442 utilizing two base-specific spin probes (Figure 1). Each bulge-
443 mismatch was simulated as a sum of FAST and SLOW
444 components (as illustrated in Figure 4) across a range of
445 temperatures in the premelting region. The temperature-depend-
446 ent results are used to determine a dynamics-based entropy and
447 enthalpy of interconversion between conformations present in
448 equilibrium within the premelting temperature region. We
449 compare our results to those of various NN model predictions
450 that are based on simple assumptions about the nature of the
451 conformations contributing to the state of the DNA as a function
452 of temperature, in the melting region. Moreover, the thermo-
453 dynamics of the conformations involved in forming the DNA
454 were examined by DSC and UV-monitored melting experiments.

EPR Reference Samples. The construct designed with a ζ
paired to \mathbf{X} ($\mathbf{X} = \mathbf{A}, \mathbf{C}, \mathbf{T},$ or \mathbf{G}), is shown in the inset of Figure
5. The melting temperatures (T_m) of each complex measured
by UV melting and EPR spectral widths measured as a function
of temperature are shown in Figure 5.

Spectral width is an established reporter of the level of spin
label motion, where the narrowest peak-to-peak line width
reflects the highest level of motion.³⁷ As seen in Figure 5, the
order of the T_m 's was $\zeta/\mathbf{G} \gg \zeta/\mathbf{A} > \zeta/\mathbf{T} > \zeta/\mathbf{C}$. Over the entire
premelting region examined, the widest spectral widths are
observed for sequences with a ζ/\mathbf{C} or ζ/\mathbf{T} , while the ζ/\mathbf{G} and
 ζ/\mathbf{A} sequences show more motion. Interestingly, the level of
motion does not correlate with the order of T_m 's, revealing that
reduced motion does not imply a more thermodynamically stable
state. On the basis of spectral width measurements, the level of
motion among the ζ/\mathbf{X} samples is lowest for ζ/\mathbf{C} , although

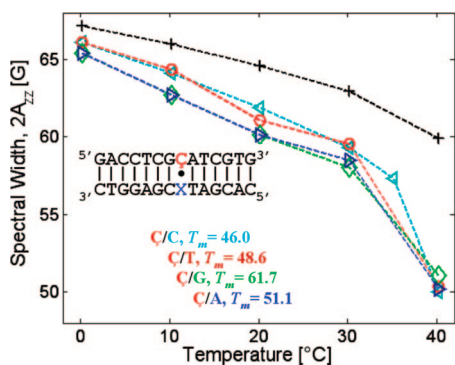


Figure 5. Spectral widths as a function of temperature, labeled with the sample name and the sample melting temperature (T_m). Sequence of constructs shown as inset, where X = A, C, T, or G. C/A (blue right-pointing triangles), C/G (green diamonds), C/T (red circles), C/C (cyan left-pointing triangles), and simulated spectra of 14-mer with no internal motion (black plus marks). Margin of error is within the size of the markers used. Dotted lines added to aid the eye.

485 C/G has a T_m that is ~ 16 °C higher than C/C. For comparison,
 486 the spectral widths of the simulated spectra are also plotted
 487 versus temperature in Figure 5. The simulations were done
 488 assuming only rigid body motion of a cylinder-like object; no
 489 internal motion was included in the calculation. Consequently,
 490 the simulated spectra have a larger spectral width than C/C,
 491 which in turn has a larger spectral width than that of a bulged
 492 C in the FAST control (spectra shown in Figure S2, Supporting
 493 Information).

494 In Figure 6 (top), the spin–lattice relaxation rates (R_{1e}) are
 495 reported for the C/X samples and the simulated 14-mer (solid
 496 blue line and plus marks) as shown in Figure 5, as well as the
 497 C-labeled bulge samples (structures shown in Figures 2 and
 498 3-IV). The solid black line indicates the excellent linear
 499 correlation between spectral width and R_{1e} for the C/X samples.
 500 The dashed black line indicates a different linear correlation
 501 between spectral width and R_{1e} for the bulged samples. The R_{1e}
 502 values, calculated on the basis of a rigid 14-mer,^{39,53} demonstrate
 503 that the experimental R_{1e} values are about twice as large as the
 504 calculated values. The increased rate of experimental values
 505 arises from the internal motion of the spin probe over and above
 506 that of a rigid object.³⁹ The R_{1e} , like the spectral width ($2A_{zz}$),
 507 indicates C/C has the least mobility of the C/X samples. Figure
 508 6 (bottom) indicates high correlation between the dynamics
 509 reported based on central field manifold measurement and full
 510 spectral width measurement.

511 Because C/C (I in Figure 3) reported the lowest level of spin
 512 label motion, it was used as a reference sample for SLOW
 513 dynamics. Control sample IV in Figure 3 has a C spin probe
 514 present without any partner available for pairing, and has a
 515 higher T_m than any of the other bulge samples (and it is nearly
 516 equal to the T_m of G/C/G), as can be seen in Table 1.

517 To show a comparison of experimental spectra from the
 518 reference constructs to spectra that are simulated with no internal
 519 motion, EPR spectra from the simulated 14-mer (first column)
 520 and the control samples I (second column), and IV (third
 521 column) at 0, 20, and 40 °C are shown in Figure S2 in
 522 Supporting Information. Sample I resembles the 14-mer rigid
 523 simulation more closely than does sample IV.

524 **A Single Base Bulge Adjacent to a Single Base Mismatch.**
 525 The EPR spectra for the bulge-mismatches at each temperature
 526 were fit to a superposition of the control spectra, and the
 527 percentage of FAST component was determined. These values
 528 are plotted versus temperature in Figure 7 (top). G/C/T, C/A/C,
 529 and G/Q/P all contain a larger percentage of the FAST spectra

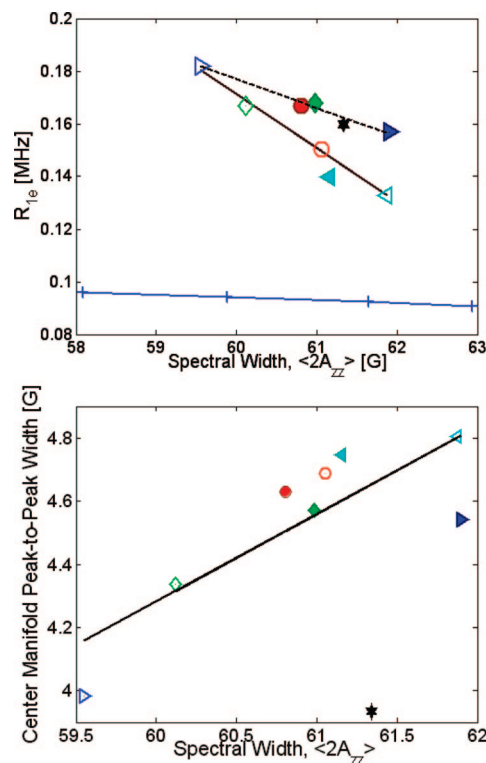


Figure 6. Top: Correlation of full spectral width at 20 °C of the C-labeled samples to the spin–lattice relaxation rate, R_{1e} , at ~ 21 °C. Solid black line is a least-squares linear fit to the nonbulged sequence data, and dashed black line is a least-squares linear fit to C/A, G/C/T, G/C/G, FAST reference IV, and G/C/A. Solid blue line with plus marks indicate the correlation of the calculated values from simulated spectra of 14-mer with no internal motion. Bottom: Correlation of center manifold peak-to-peak line width and spectral width, both measured at 20 °C. G/C/A (solid blue right-pointing triangle), C/A (hollow blue right-pointing triangle), G/C/G (solid green diamond), C/G (hollow green diamond), G/C/T (solid red circle), C/T (hollow red circle), C/A/C (solid cyan left-pointing triangle), C/C (hollow cyan left-pointing triangle), and FAST reference IV (solid black star). Solid black line is a least-squares linear fit to all data points except the FAST reference.

530 at higher temperature, G/C/A is fairly constant across the
 531 temperature range studied, and G/C/G and Q/A/P both have less
 532 FAST at higher temperature.

533 Using eq 1.2 and results of fitting the EPR spectra to a
 534 superposition of the two controls, $\ln(K_{eq})$ at each temperature
 535 and for the different samples was determined, and plotted versus
 536 $[1/T]$ in Figure 7 (bottom). Points were fit to the van't Hoff
 537 equation and values of ΔH_D and ΔS_D were derived, and are
 538 listed in Table 2. G/C/A, G/C/T, C/A/C, and G/Q/P all have
 539 endothermic SLOW→FAST transitions, while G/C/G and Q/A/P
 540 both have exothermic SLOW→FAST transitions. The ΔH_D and
 541 ΔS_D values in Table 2 were used to calculate $\Delta G_D(T)$ of the
 542 interconversion at 20 °C given in Table 2.

543 The spectra from bulge-mismatch samples G/C/A, G/C/G,
 544 G/C/T and C/A/C (structures shown in Figure 2) were fit as a
 545 sum of the FAST reference IV and the corresponding spectra
 546 from the C/X samples. For example, G/C/T was fit to a sum of
 547 FAST and C/T. Results are shown in Figure S3 in Supporting
 548 Information. Comparing the plots in Figures 7 (top) and S3
 549 (Supporting Information), it is evident that the results obtained
 550 when using the closest-matching C/X as reference spectra are
 551 not qualitatively different than when C/C is used as the reference
 552 SLOW sample. Therefore, using the C/C construct as general
 553 reference sample, rather than use a construct specific for a
 554 particular sequence, does not compromise any of the conclusions.

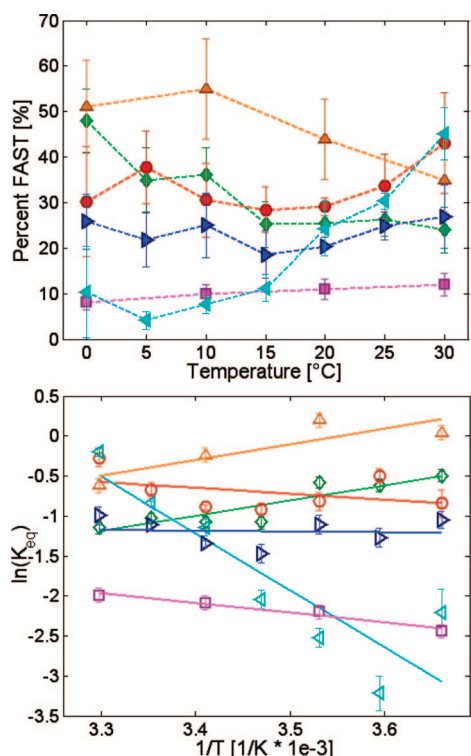


Figure 7. Top: Results of fitting spectra to a sum of SLOW spectra and FAST spectra, as a function of temperature. Dotted lines are added to aid the eye. Bottom: Plot illustrating $\ln(K_{eq})$ versus $1/T$ [$1/K$], where K_{eq} is calculated from spectral fitting, as shown in eq 1.2. $G\zeta/A$ (blue right-pointing triangles), $G\zeta/G$ (green diamonds), $G\zeta/T$ (red circles), $\zeta A/C$ (cyan left-pointing triangles), GQ/P (purple squares), and QA/P (orange triangles) sequences.

TABLE 2: Thermodynamic Data for the Interconversion SLOW—FAST, Derived from the EPR Data

sample	ΔH_D [kcal/mol]	ΔS_D [cal/mol]	ΔG_{20} [kcal/mol]
$G\zeta/A$	$+0.2 \pm 1.0$	-1.5 ± 3.5	$+0.7 \pm 1.2$
$G\zeta/G$	-3.8 ± 0.7	-15.0 ± 2.5	$+0.6 \pm 0.9$
$G\zeta/T$	$+1.4 \pm 1.3$	$+3.6 \pm 4.4$	$+0.4 \pm 1.5$
$\zeta A/C$	$+14.2 \pm 2.9$	$+45.7 \pm 10$	$+0.8 \pm 3.2$
GQ/P	$+2.4 \pm 0.3$	$+4.0 \pm 0.9$	$+1.2 \pm 0.6$
QA/P	-3.9 ± 1.2	-13.9 ± 4.1	$+0.2 \pm 1.4$

A Single Base Bulge Adjacent to Two Mismatched Basepairs. To demonstrate the complex equilibria present in $G\zeta A/AC$, samples $G\zeta A$, $\zeta A/C$, and $G\zeta A/AC$ (shown in Figure 2) were fit to a spectral sum of SLOW and FAST control spectra. For sample $G\zeta A/AC$, any of the three center bases (G , ζ , or A) could form a one-base bulge, which leaves the neighboring bases to form two mismatched basepairs. Among the many possibilities for dominant structures, there are likely two competing equilibria in $G\zeta A/AC$: (1) The competition between the G and ζ for the A mismatch, and (2) the competition between the ζ and A for the C mismatch. The former is much like the $G\zeta A$ construct and the latter is much like the $\zeta A/C$ construct, which have been analyzed by the same SLOW to FAST equilibrium.

Results of fitting $G\zeta A/AC$, $G\zeta A$, and $\zeta A/C$ to a sum of the spectra for the controls **I** and **IV** are shown in Figure 8. From 5–20 °C, the percentage of the FAST component in $G\zeta A/AC$ correlates with that of $G\zeta A$. From 20–35 °C it switches to matching the data of $\zeta A/C$. Because the EPR-based data for $G\zeta A/AC$ was not monotonically linear, the van't Hoff analysis could not be applied to derive a ΔH_D and ΔS_D for the conformational interconversion in these complex equilibria.

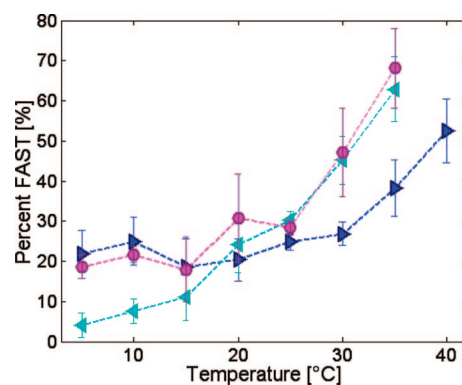


Figure 8. A comparison of a sample that has two possible bulge-mismatch equilibria, $G\zeta A/AC$, (magenta circles), with bulge-mismatch results on each of the two equilibria individually: $\zeta A/C$ (cyan left-pointing triangles) and $G\zeta A$ (blue right-pointing triangles).

Similarity between the fraction of the $G\zeta A/AC$ sequence and the two single base bulges in the two different temperature regimes, suggests the equilibrium is composed of multiple interconverting structures, which differ markedly with temperature.

Melting Thermodynamics for Bulge-Mismatches. Thermodynamic parameters evaluated by UV and DSC melting curve analysis are summarized in Tables 1 and 3. The ΔH_f and ΔS_f from UV melting studies are all more negative than the DSC results, as are the resultant ΔG_f values at 20 °C. As expected, the T_m values obtained by UV melting experiments are 10–21 °C lower than measured by DSC for every sample. This difference in T_m was most certainly due to the difference in concentrations for the two types of experiment.

From calorimetry, the order of thermal stability (as determined by either the T_m 's or the enthalpies of melting, except for the problematic ζ/C) is $\zeta/G > \zeta/A > \zeta/T > \zeta/C$. This order of thermodynamic stability may be compared with the order of dynamics; of these four constructs ζ/C show the slowest dynamics and ζ/G has the fastest dynamics. Therefore the orders do correlate; however, the orders are counter to the notion that the most thermodynamically stable entities will have the slowest motion. Below we discuss why the dynamics of structures in the premelt region need not correlate with thermal stability. For the bulge-mismatch samples, the order of enthalpic stability is $G\zeta/G > G\zeta/T > G\zeta A > \zeta A/C$, based on UV melting and assuming a two-state model for all samples (Table 1). This set of constructs is compared because it represents a series in which ζ is opposite each of the four bases, as the ζ/X series. The order of thermodynamic stability of the bulge-mismatches is nearly the same as the corresponding oligomers in the ζ/X series. The data in Figure 7 (derived from the EPR spectra) show that in the premelt region, the nature of the structure is not explained by either the SLOW (ζ/X pairing) or the FAST construct alone. The UV melting curves for samples $\zeta A/C$ and ζ/C were broadened and have a slight shoulder toward higher temperature that provides direct calorimetric evidence that makes the two-state model even more questionable.

The DSC data in Table 3 for $G\zeta A$ and $G\zeta A/AC$ (the bulge-double mismatch) are remarkably similar, although the UV melting data for these two samples did not show the same high level of similarity. In fact, the UV melting data showed nearly identical results for $\zeta A/C$ and $G\zeta A/AC$. A comparison of DSC results for $G\zeta A/AC$ and $\zeta A/C$ cannot be made because the $\zeta A/C$ molecule displayed two distinct peaks in the DSC melting curve. Other DSC curves of 14-mer and 11-mer bulge-single mismatch constructs having a C/C interaction as one conformational possibility also showed two peaks (data not shown).

555
556
557
558
559
560
561
562
563
564
565
566
567
568
569
570
571
572
573
574
575
576

577
578
579
580
581
582
583
584
585
586
587
588
589
590
591
592
593
594
595
596
597
598
599
600
601
602
603
604
605
606
607
608
609
610
611
612
613
614
615
616
617
618
619
620
621
622
623

TABLE 3: Results of DSC Measurements^a

sample	ΔH_f [kcal/mol]	ΔS_f [cal/mol]	$\Delta G_{f, 20}$ [kcal/mol]	T_m [°C]
SLOW, I	-86.9 ± 1.1	-249 ± 4	-13.9 ± 0.1	77.1 ± 0.1
FAST, IV	-83.8 ± 3.6	-248 ± 11	-11.1 ± 0.5	65.4 ± 0.1
G \bar{C} /G (GC/G)	-71.4 ± 0.7	-213 ± 2	-8.9 ± 0.2	61.6 ± 0.1
G \bar{C} /T (GC/T)	-69.2 ± 2.1	-210 ± 6	-7.6 ± 0.2	56.0 ± 0.2
G \bar{C} /A (GC/A)	-68.8 ± 1.6	-208 ± 5	-7.8 ± 0.2	57.9 ± 0.2
\bar{C} A/C (CA/C)	<i>b</i>	<i>b</i>	<i>b</i>	46.7 ± 0.2
				65.3 ± 0.2
G \bar{C} A/AC (GCA/AC)	-68.6 ± 2.8	-209 ± 9	-7.3 ± 0.2	54.4 ± 0.1

^a SLOW represents the thermodynamic values for the SLOW control sample that is the top structure in Figure 3, and FAST is the FAST control sample for the top construct in Figure 4. Instead of a spin probe, a natural cytidine base is used at the site of the spin probe, as shown in the parenthesis. ^b The enthalpy and entropy could not be obtained from the DSC curves for this sample, as there were two distinct peaks in the data, each of which had a unique T_m .

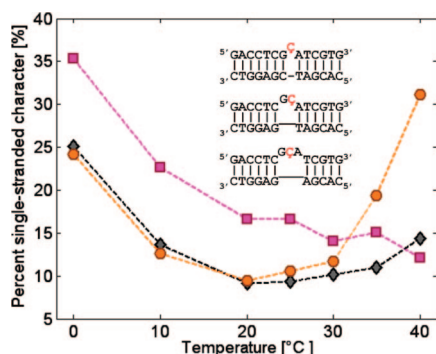


Figure 9. Results of fitting one- (purple squares), two- (black diamonds), and three-base (black orange circles) (structures shown in inset) bulge spectra to a sum of single- and double-stranded character (SLOW control I). The single-stranded reference comes from spectra of the spin-labeled 14-mer used in SLOW control I with no complementary strand. Error margins for each data point are <5%. (T_m s are 46.8 °C for the one-base bulge, 35.8 °C for the two-base bulge, and 27.0 °C for the three-base bulge.)

Comparison of EPR Experimental Data to NN Calculations. Results of the EPR-derived thermodynamics of interconversion from SLOW→FAST were compared for two different types of NN calculations in Figure S4 in Supporting Information. No clear correspondence was observed between EPR-derived thermodynamics and the analogous parameters from the NN calculations.

In order to observe whether the calorimetric data corresponded with NN calculation, the experimentally derived DSC and UV melting values for enthalpy and entropy of formation were compared directly to the NN-calculated thermodynamics of formation for either the FAST or SLOW state. Figure S5 in Supporting Information shows that this method of comparing calorimetric data to NN calculations for bulge-mismatches is an inadequate means of determining the conformations.

EPR Studies Comparing One-, Two-, and Three-Base Bulges. EPR spectra for one-, two-, and three-base bulge samples (inset of Figure 9) were fit to a spectral sum of the spectrum of I (Figure 3) and the single 14-mer spin-labeled strand used to make I without any complementary strand. The fitting method was the same as used for the bulge-mismatches, except the single-strand served as the FAST control. Results of the spectral fitting are shown in Figure 9. From 0 to 30 °C, the one-base bulge displays the most single-strand character (highest level of motion). The two- and three-base bulges reported nearly identical results from 0 to 20 °C. Above 20 °C, the three-base bulge began to show more and more single-strand character, presumably because it has the fewest paired bases, more conformational freedom of the bulged region, and melts at a

lower temperature (27.0 °C for the three-base bulge as compared to 35.8 °C for the two-base bulge) as determined by UV melting.

Discussion

These studies have shown that a base-specific probe in conjunction with a spectroscopic technique can provide information not attainable by melting studies. EPR spectroscopy is a valuable technique for such studies, since it is sensitive to dynamics on the nanosecond to microsecond time scale. Thus, EPR is suitable for observing local motions in DNA, (as well as twisting and bending collective motions and overall tumbling motions for nucleic acids).⁴² EPR studies of nucleic acids require incorporation of unpaired electrons, such as nitroxide radicals. For detection of base or nucleotide specific dynamics, the nitroxide spin labels must be somewhat rigid, that is not have motion independent of the nucleotide to which they are attached.

The spin labels in this study have been base-specifically attached within the helical structure of the DNA constructs; therefore, they provide information about the local structure and environment of the labeled base through the dynamics of the spin probe. The EPR spectra reflect less motion when the spin label is firmly locked within the duplex structure relative to when the spin label is bulged out or otherwise not held tightly. In this way, the dynamic's signatures of the spin probe reflect the equilibrium among possible structures. The EPR-based information is complementary to standard thermodynamic data, because it indicates which possible structures are present under conditions of thermodynamic equilibrium. We present here the type of information that can be obtained from such probes, and provide a framework to understand the information and compare it with DSC results and calculations using the NN model. Our results indicate that in the premelting region at a fixed pressure and temperature the DNA is composed of several different structures.

Both UV and DSC melting data (Tables 1 and 3, Figure S5 in Supporting Information) indicate formation of bulge-mismatches is a nontwo-state process. Origins of the differences of a van't Hoff-derived (UV melting) ΔH_f and the model-independent (DSC) ΔH_f have been discussed by Breslauer and co-workers.²⁹ Results presented here consistently showed the van't Hoff-derived ΔH_f was less than the calorimetric ΔH_f , highly indicative of a nontwo-state process of formation.²⁹ This nontwo-state formation has been observed by others, particularly in DNA duplexes with noncanonical Watson–Crick sites.⁵⁴ The structural evaluations determined by site-specific EPR probes distinguish among possible structures that are present prior to melting. The data show that bulge-mismatch DNA in the premelting region is composed of at least two distinct conformations. Comparison of results from NN calculations with EPR

701 data for the thermodynamics of structural interconversion is
 702 tenuous because the EPR results are determined directly from
 703 a base-specific probe, which reports on structure in the pre-
 704 melting region through a dynamics-dependent parameter, while
 705 the NN model is based on thermodynamic parameters from
 706 changes around the melting transition region.

707 There are two potential points worth consideration when
 708 applying the NN model to calculate stabilities of somewhat
 709 unusual duplexes, containing bulges and mismatches, at tem-
 710 peratures below the melting transition. First is the validity of
 711 the NN model for these types of structures. It is likely that the
 712 effects of single base bulges extend beyond the nearest neighbor
 713 base pairs. Second, throughout our analysis it has been assumed
 714 that the excess heat capacity difference between helical and
 715 coiled states is zero [$\Delta C_p = 0$] (i.e., that the enthalpy and entropy
 716 evaluated from DSC melting curves are temperature independ-
 717 ent). If correct, then predicted thermodynamics at temperatures
 718 well below the transition temperature should be accurate.
 719 However, if ΔC_p does not equal zero, then the enthalpy and
 720 entropy are temperature dependent. This would imply thermo-
 721 dynamic parameters evaluated from analysis of the melting
 722 transition region may not be accurate when extrapolated to
 723 temperatures in the pretransition temperature region. The
 724 likelihood of polymorphic states occupied by the duplex and
 725 potential temperature dependence of the thermodynamic pa-
 726 rameters cast suspicion on reliability of results and comparisons
 727 based on the NN model.

728 For the samples spin-labeled with ζ , the control SLOW
 729 duplex has a cytidine across from the ζ spin label. This ζ/C
 730 sample was chosen as the reference because this particular
 731 sample give spectra that contain the least amount of EPR-
 732 observable dynamics. Surprisingly, the ζ/C construct is the most
 733 rigid dynamically but had the lowest T_m . Reduced motion of
 734 ζ/C compared to the other ζ/X samples inversely correlates
 735 with the thermodynamic stability. The order of T_m 's (Figures 7
 736 and 8 and Tables 1 and 3) demonstrates that thermal stability
 737 is opposite to dynamic stability.

738 The motion observed from the spin probe consists of two
 739 types: the uniform motion of the duplex DNA and the internal
 740 motions of the probe relative to the duplex. Figures 4 and 5
 741 (top) and Figure S2 in Supporting Information provide a
 742 comparison of the experimental data with simulations of what
 743 the results would look like if only the uniform modes of motion
 744 were present. The comparisons show that the SLOW spectra
 745 are indeed closer to the uniform mode-only spectra than are
 746 the bulge-mismatches (Figure 6 (top)), and even the SLOW
 747 motion spectra contain local dynamics in addition to the uniform
 748 modes of motion (Figure 5).

749 Figure 6 illustrates different possible ways to measure a
 750 dynamic signature from the spin probe attached to a single base.
 751 The three parameters are (1) the full spectral splitting, called
 752 $2\langle A_{zz} \rangle$, (2) the central line width, which is directly related to
 753 the mobility parameter of Hubbell,³⁸ and (3) the spin lattice
 754 relaxation rate, R_{1e} .³⁹ Each parameter depends on the dynamics
 755 in different ways. However, all three track the dynamics
 756 qualitatively in the same way. The R_{1e} measurement follows
 757 $2\langle A_{zz} \rangle$ linearly, when the character of the dynamics is held
 758 constant (Figure 5). For example, R_{1e} of the 4 ζ/X structures
 759 show a simple linear relation with $2\langle A_{zz} \rangle$, and the bulged
 760 structures show a different linear relation. This illustrates that
 761 R_{1e} depends on the dynamics in a different way from the $2\langle A_{zz} \rangle$
 762 and when the characteristics of the motion change the relation
 763 changes.

764 The comparison of the spin–lattice relaxation rate, R_{1e} , with
 765 the CW EPR spectral width, $2\langle A_{zz} \rangle$ (Figure 6 (top)), provides
 766 information on the origin of the dynamics. As a general
 767 principle, $2\langle A_{zz} \rangle$ is determined in main part by dynamics
 768 processes that have rotational diffusion coefficients comparable
 769 to the width of the spectrum, which is on the order of 10^8 Hz.
 770 In contrast, the R_{1e} is dominated by dynamics process that
 771 compete with the spectrometer frequency, which is 9×10^9 Hz
 772 (for X-band spectrometers).^{39,53,55} Therefore, the results from
 773 the simulated spectra (Figure 6 (top), blue line) demonstrate
 774 that R_{1e} for a sample with no internal motion does not depend
 775 strongly on the uniform mode of motion of the spin label, as
 776 the uniform mode for a ~ 14 -mer is much slower than the
 777 spectrometer frequency. However, the strong correlation of R_{1e}
 778 relative to $2\langle A_{zz} \rangle$ for the ζ/X and bulge-mismatch samples (black
 779 and dashed black lines in Figure 6 (top)) indicates that R_{1e} is
 780 sensitive to rapid motion, which is the motion of the base relative
 781 to the local helical structure. The dominant dynamics do not
 782 come from the collective modes. The collective modes are nearly
 783 independent of sequence; however, both experimental dynamics
 784 signatures are quite sensitive to sequence. Moreover, for such
 785 short lengths of DNA the amplitudes of such modes are very
 786 small. Experimentally, the rapid local dynamics are so fast that
 787 the rate of the motion does not affect $2\langle A_{zz} \rangle$, although the
 788 amplitude of the local motion likely does affect the width. The
 789 experimental data of the set of ζ/X samples (solid black line
 790 in Figure 6 (top)) as compared to the set of bulge-mismatches
 791 (dashed black line in Figure 6 (top)) shows each set spans a
 792 similar range of values of $2\langle A_{zz} \rangle$. This indicates that the range
 793 of amplitudes of motion is similar in the two types of structures.
 794 However, the range of R_{1e} values is larger for the ζ/X construct
 795 set than for the bulge-mismatch set, which indicates that the
 796 rates of motion for the bases within the helix are faster (i.e.,
 797 closer to the spectrometer frequency) than those in the bulges.
 798 Therefore, having two independent dynamics signatures allows
 799 us to identify the local motion, including both the rate and the
 800 amplitude of motion, that contribute to defining the different
 801 states of the DNA.

802 From a structural perspective, differences in dynamics reflect
 803 the possibility that the pyrimidine-based spin label ζ , when
 804 paired with a pyrimidine, either cytidine or thymidine, does not
 805 fill the region of space in the center of the duplex to the extent
 806 that ζ paired with either purine does. Hence the equilibrium
 807 structure of ζ , when paired with a pyrimidine, is that of a
 808 basepair held further within the helix, and thus the spin probe
 809 appears more rigidly locked by the surrounding duplex.
 810 Therefore, while the ζ/C pairing in the duplex is thermody-
 811 namically less stable than the ζ/G pairing, it appears to be
 812 dynamically more rigid. The present observations of a close
 813 ζ/C interaction agree with other proposed structure(s) for the
 814 C/C pairing and with reported thermodynamic instability in the
 815 melting region in DNA duplexes with C/C pairings.^{54,56} It was
 816 also reported that perturbations induced by C/C pairing may
 817 persist over several base pairs.^{54,56} It is difficult to clearly define
 818 the extent or range of this interaction by conventional thermo-
 819 dynamic methods such as DSC. However, as shown here, EPR
 820 spectroscopy may provide an alternate viewpoint from which
 821 to investigate such sequence dependent perturbative effects.
 822 Consequently, our results on stability of ζ/C in the premelting
 823 region underscores the distinction between the information
 824 obtained from analysis of the melting region and that obtained
 825 from the EPR dynamics-sensitive base probe in the premelting
 826 region.

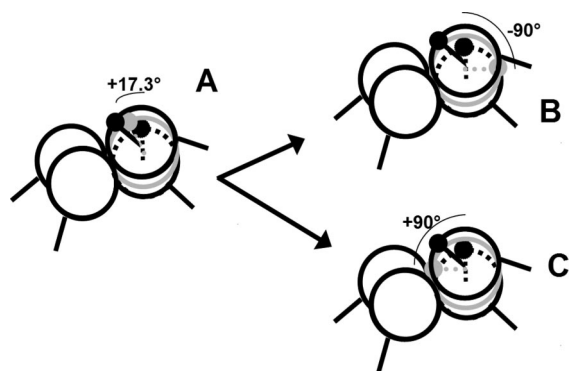


Figure 10. Cartoon-style figures of a bulged base, (2 in Figure 9), at different positions with respect to the duplex and interelectron distances from a neighboring base in the duplex. The neighboring base is considered to be at the back in these depictions. (A) Two possible orientations and distances for the bulged base, as referenced to the previous base: $+17.3^\circ$ and 1.7 \AA from the neighboring base (gray), versus 34.6° and 3.4 \AA (black), a usual base step. (B) A -90° rotation of an unpaired base. (C) A $+90^\circ$ rotation of an unpaired base.

Validity of our assumptions on the structures of the SLOW and FAST references as well as bulge-mismatches is demonstrated by examining the distances between two Q probes. By determining the distance between two neighboring Q probes in duplex form, the spectrum (Figure S6 in Supporting Information [1]) shows that nearest neighbor Q's are at the interelectron distance predicted by simple helical B-form DNA (7.2 \AA).⁵⁷ When one Q probe is in a bulged position, the distance between the two Q's is that of one probe pushed out of the helix and rotated, as illustrated in Figure 10. On the left in Figure 10, the bulged base is shown stacked into the duplex without a partner, sandwiched in between neighboring base pairs with a rotation angle of 17.3 degrees (half of the 34.6 degrees for a normal rotation) and a height of 1.7 \AA . The predicted distance between the two spin probes, based on this geometry, would be only $\sim 5 \text{ \AA}$. Rotating the extra base by either 90° inward (B) or 90° outward (C), from the preceding base leads to distances of $\sim 11 \text{ \AA}$, which though structurally unlikely, corresponds to the distance measured between the neighboring spins. This result supports the assertion that one spin label is bulged out and rotated, likely with some additional bending, while the other remains locked into the helical structure.

Figure 9 shows that the one-base bulge FAST reference does not appear to intercalate into the duplex, as evidenced by the large percentage of single stranded dynamics. However, the two- and three-base bulge sequences seem to stabilize and be more like the duplex forms. One possible explanation for why the larger bulged region might appear to have less dynamics is that the bases stack but remain looped out. Other studies have suggested that the presence of stacked bases generates a local bend in the duplex DNA.⁵⁸ For the case of one-, two-, and three-base adenine bulges the adenines stack into the duplex.²⁷ The basepairs on either side of the bulge remains intact, but as the number of adenines at the bulge site increases, the bending increases.²⁷ A solution NMR structure of an A-T-A 3-base bulge within a 12-mer DNA oligonucleotide showed that three bases did not greatly disrupt the helical axis but rather created a large twist or "lateral shearing" between the two halves of the duplex.⁵⁸ The present results seem to be very much in agreement with these other findings. The bulge-mismatches observed here are that of a stacked set of bases on the bulge side which neither intercalate nor directly stack against the duplex structure.

In Figure 8, the analysis of G ζ A/AC in terms of the SLOW and FAST references demonstrates a complicated dependence

on temperature that cannot be modeled by a simple two-state van't Hoff type analysis. Nonetheless, a comparison with the two constructs G ζ A and ζ A/C reveals startling similarities. At low temperature (below 20°C), the G ζ A/AC construct is much like one possible component, the G ζ A construct, and at higher temperatures, is more like the other possible component, the ζ A/C construct. It is not surprising that the high temperature form is the one that is more calorimetrically similar to the G ζ A/AC construct as it is the dominant form leading into the melting region. The conclusion about the G ζ A/AC construct is that it is a temperature-dependent bistable structure, which approximates one type of bulge-mismatch equilibrium at low temperatures (the G ζ A form, Figure 2) and another type at high temperatures (the ζ A/C form, Figure 2). Moreover, each of the components of this bistable switching structure (the G ζ A and the ζ A/C constructs) is in turn composed of multiple-conformations.

Conclusions

Local, base-specific probes can provide dynamics and structural information on the nature of the components involved in polymorphic nucleic acid structures where nonduplex forms, specifically bulges and mismatches, are involved. Structural information can be obtained from different EPR-based "dynamic signatures". Two different base-specific probes were used in multiple bulge-mismatch constructs, and van't Hoff analysis was used to examine the thermodynamics. Neither probe yielded a clear correspondence with NN model calculations. The utility of a base-specific probe to complement and interpret complex calorimetric data on multistate structures has been demonstrated. The presence of several states in the premelt region of a bulge-mismatch structure is demonstrated; therefore, the calorimetric data on these structures cannot be interpreted in terms of a simple two-state model. Through analysis of the dynamics of a base-specific spin probe, we are able to demonstrate that a multistate structure can be analyzed in terms of simpler bulges, and that temperature dependent, bistable forms may be quite common in nonduplex DNA and by implication RNA.

Acknowledgment. This work was supported in part by NIH GM65944, GM62360, and NIH-NIEHS P30ES07033, the Iceland Research Fund (60028021), and by a doctoral fellowship to P.C. from the Eimskip Fund of the University of Iceland. The authors thank Steve Alley for assistance in sample preparation, Kari Pederson, Greg Olsen, and Dorothy Caplow Echodu for comments on the manuscript, and J. Michael Schurr for scientific insight.

Supporting Information Available: Figures illustrating the following: two-component fit of EPR spectra; calculation of α from UV melting curves; rigid 14-mer simulated, FAST, and SLOW spectra at 0 , 20 , and 40°C ; results of fitting spectra to FAST and "closest match ζ/X " spectra; NN calculation comparisons; and spectra and analysis of doubly spin-labeled samples for distance measurements. This material is available free of charge via the Internet at <http://pubs.acs.org>.

References and Notes

- (1) Ellison, M. J.; Fenton, M. J.; Ho, P. S.; Rich, A. *EMBO J.* **1987**, *6*, 1513.
- (2) Kim, U. S.; Fujimoto, B. S.; Furlong, C. E.; Sundstrom, R.; Humbert, D.; Teller, C.; Schurr, J. M. *Biopolymers* **1993**, *33*, 1725.
- (3) Roy, K. B.; Miles, H. T. *Biochem. Biophys. Res. Commun.* **1983**, *115*, 100.
- (4) Schurr, J. M.; Delrow, J. J.; Fujimoto, B. S.; Benight, A. S. *Biopolymers* **1997**, *44*, 283.

- 933 (5) Shindo, H.; Fujiwara, T.; Akutsu, H.; Matsumoto, U.; Shimidzu,
934 M. *J. Mol. Biol.* **1984**, *174*, 221.
- 935 (6) Wang, J. C.; Davidson, N. *J. Mol. Biol.* **1966**, *15*, 111.
- 936 (7) International Human Genome Sequencing Consortium. *Nature* **2004**,
937 *431*, 931.
- 938 (8) Inglehearn, C. F.; Cooke, H. J. *Nucleic Acids Res.* **1990**, *18*, 471.
- 939 (9) Kondo, J.; Sunami, T.; Takenaka, A. *Acta Crystallogr., Sect. D*
940 **2007**, *63*, 673.
- 941 (10) Stassinopoulos, A.; Ji, J.; Gao, X.; Goldberg, I. H. *Science* **1996**,
942 *272*, 1943.
- 943 (11) McNally, E. M.; Duggan, D.; Gorospe, J. R.; Bonnemann, C. G.;
944 Fanin, M.; Pegoraro, E.; Lidov, H. G. W.; Noguchi, S.; Ozawa, E.; Finkel,
945 R. S.; Cruse, R. P.; Angelini, C.; Kunkel, L. M.; Hoffman, E. P. *Hum.*
946 *Mol. Genet.* **1996**, *5*, 1841.
- 947 (12) Hol, E. M.; van Leeuwen, F. W.; Fischer, D. F. *Trends Mol. Med.*
948 **2005**, *11*, 488.
- 949 (13) Collins, F. S.; Brooks, L. D.; Chakravarti, A. *Genome Res.* **1998**,
950 *8*, 1229.
- 951 (14) Li, N.; Mei, L.; Xiang, Y.; Tong, A.; Nishizawa, S.; Teramae, N.
952 *Anal. Chim. Acta* **2007**, *597*, 97.
- 953 (15) Okamoto, A.; Tainaka, K.; Kamei, T. *Org. Biomol. Chem.* **2006**,
954 *4*, 1638.
- 955 (16) Okamoto, A. *Nucleosides, Nucleotides, Nucleic Acids* **2007**, *26*,
956 1601.
- 957 (17) Takei, F.; Suda, H.; Hagihara, M.; Zhang, J.; Kobori, A.; Nakatani,
958 K. *Chemistry* **2007**, *13*, 4452.
- 959 (18) Cekan, P.; Sigurdsson, S. T. *Chem. Commun. (Cambridge, U.K.)*
960 **2008**, *29*, 3393.
- 961 (19) Chi, L. M.; Lam, S. L. *Biochemistry* **2008**, *47*, 4469.
- 962 (20) Shibutani, S. *Environ. Mutagen Res.* **2004**, *26*, 135.
- 963 (21) Kalnik, M. W.; Norman, D. G.; Li, B. F.; Swann, P. F.; Patel, D. J.
964 *J. Biol. Chem.* **1990**, *265*, 636.
- 965 (22) Kalnik, M. W.; Norman, D. G.; Zagorski, M. G.; Swann, P. F.;
966 Patel, D. J. *Biochemistry* **1989**, *28*, 294.
- 967 (23) Fish, D. J.; Horne, M. T.; Brewood, G. P.; Goodarzi, J. P.;
968 Alemayehu, S.; Bhandiwad, A.; Searles, R. P.; Benight, A. S. *Nucleic Acids*
969 *Res.* **2007**, *35*, 7197.
- 970 (24) Kalnik, M. W.; Norman, D. G.; Swann, P. F.; Patel, D. J. *J. Biol.*
971 *Chem.* **1989**, *264*, 3702.
- 972 (25) Nikonowicz, E. P.; Meadows, R. P.; Gorenstein, D. G. *Biochemistry*
973 **1990**, *29*, 4193.
- 974 (26) Popenada, L.; Adamiak, R. W.; Gdaniec, Z. *Biochemistry* **2008**, *47*,
975 5059.
- 976 (27) Rosen, M. A.; Live, D.; Patel, D. J. *Biochemistry* **1992**, *31*, 4004.
- 977 (28) Wang, Y.; Patel, D. J. *Biochemistry* **1995**, *34*, 5696.
- 978 (29) Breslauer, K. J. *Methods Enzymol.* **1995**, *259*, 221.
- 979 (30) Crothers, D. M.; Zimm, B. H. *J. Mol. Biol.* **1964**, *9*, 1.
- 980 (31) DeVoe, H.; Tinoco, I., Jr. *J. Mol. Biol.* **1962**, *4*, 500.
- 981 (32) SantaLucia, J., Jr. *Proc. Natl. Acad. Sci. U.S.A.* **1998**, *95*.
- 982 (33) Barhate, N.; Cekan, P.; Massey, A. P.; Sigurdsson, S. T. *Angew.*
983 *Chem., Int. Ed.* **2007**, *46*, 2655.
- (34) Miller, T. R.; Alley, S. C.; Reese, A. W.; Solomon, M. S.;
984 McCallister, W. V.; Mailer, C.; Robinson, B. H.; Hopkins, P. B. *J. Am.*
985 *Chem. Soc.* **1995**, *117*, 9377.
- (35) Cekan, P.; Smith, A. L.; Barhate, N.; Robinson, B. H.; Sigurdsson,
986 S. T. Rigid spin-labeled nucleoside C: A non-perturbing EPR probe of
987 nucleic acid conformation. *Nucleic Acids Res.*, in press.
- (36) Nielsen, R.; Canaan, S.; Gladden, J. A.; Gelb, M. H.; Robinson,
988 B. H. *J. Magn. Reson.* **2004**, *169*, 129.
- (37) Freed, J. H. *Theory of slow tumbling ESR spectra for nitroxides.*
989 *In Spin Labeling: Theory and Applications*; Berliner, L. J., Ed.; Academic
990 Press: New York, 1976; p 53.
- (38) Columbus, L.; Hubbell, W. L. *Trends Biochem. Sci.* **2002**, *27*, 288.
- (39) Smith, A. L.; Cekan, P.; Rangel, D. P.; Sigurdsson, S. T.; Mailer,
991 C.; Robinson, B. H. *J. Phys. Chem. B* **2008**, *112*, 9219.
- (40) Griffith, O. H.; Jost, P. C. *Lipid Spin Labels in Biological*
992 *Membranes. In Spin Labeling: Theory and Applications*; Berliner, L. J.,
993 Ed.; Academic Press, Inc.: New York, 1976; Vol. 1; p 453.
- (41) Freed, J. H.; Fraenkel, G. K. *J. Chem. Phys.* **1963**, *39*, 326.
- (42) Okonogi, T. M.; Reese, A. W.; Alley, S. C.; Hopkins, P. B.;
994 Robinson, B. H. *Biophys. J.* **1999**, *77*, 3256.
- (43) Tirado, M. M.; Torre, J. G. d. l. *J. Chem. Phys.* **1980**, *73*, 1986.
- (44) Okonogi, T. M. Dynamics, thermodynamics, and structural investiga-
995 tions of nucleic acids using site-specific spin-labeling and electron
996 paramagnetic resonance, University of Washington, 2000.
- (45) SantaLucia, J. J.; Hicks, D. *Annu. Rev. Biophys. Biomol. Struct.*
997 **2004**, *33*, 415.
- (46) Law, S. M.; Eritja, R.; Goodman, M. F.; Breslauer, K. J.
998 *Biochemistry* **1996**, *35*, 12329.
- (47) Ricelli, P. V.; Vallone, P. M.; Kashin, I.; Faldasz, B. D.; Benight,
999 A. S. *Biochemistry* **1999**, *38*, 11197.
- (48) Vallone, P. M.; Benight, A. S. *Biochemistry* **2000**, *39*, 7835.
- (49) Chalikian, T. V.; Volker, J.; Plum, G. E.; Breslauer, K. J. *Proc.*
1000 *Natl. Acad. Sci. U.S.A.* **1999**, *96*, 7853.
- (50) Jelesarov, I.; Crane-Robinson, C.; Privalov, P. L. *J. Mol. Biol.* **1999**,
1001 *294*, 981.
- (51) Privalov, P. L.; Jelesarov, I.; Read, C. M.; Dragan, A. I.; Crane-
1002 Robinson, C. J. *J. Mol. Biol.* **1999**, *294*, 997.
- (52) Holbrook, J. A.; Capp, M. W.; Saecker, R. M.; Record, M. T. J.
1003 *Biochemistry* **1999**, *38*, 8409.
- (53) Mailer, C.; Nielsen, R.; Robinson, B. H. *J. Phys. Chem. A* **2005**,
1004 *109*, 4049.
- (54) Tikhomirova, A.; Beletskaya, I. V.; Chalikian, T. V. *Biochemistry*
1005 **2006**, *45*, 10563.
- (55) Robinson, B. H.; Haas, D. A.; Mailer, C. *Science* **1994**, *263*, 490.
- (56) Boulard, Y.; Cognet, J. A. H.; Fazakerley, G. V. *J. Mol. Biol.* **1997**,
1006 *268*, 331.
- (57) Hustedt, E. J.; Smirnov, A. I.; Laub, C. F.; Cobb, C. E.; Beth, A. H.
1007 *Biophys. J.* **1997**, *72*, 1861.
- (58) Rosen, M. A.; Shapiro, L.; Patel, D. J. *Biochemistry* **1992**, *31*, 4015.